International Journal of Modern Physics E
(2022) 2240001 (10 pages)

DOI: 10.1142/S0218301322400018

World Scientific
www.worldscientific.com

Investigation of the low-energy K^- hadronic interactions with light nuclei by AMADEUS

Magdalena Skurzok[*,†,***], Massimiliano Bazzi[†], Mario Bragadireanu[‡], Damir Bosnar[§], Michael Cargnelli[¶], Alberto Clozza[†], Catalina Curceanu[†], Luca de Paolis[†,‖], Raffaele Del Grande[**,†,††], Laura Fabbietti[**,‡‡], Carlo Guaraldo[†], Mihai Iliescu[†], Masahiko Iwasaki[§§], Paolo Levi Sandri[†], Johann Marton[¶], Marco Miliucci[†,‖], Pawel Moskal[*], Kristian Piscicchia[†,††], Angels Ramos[¶¶], Alessandro Scordo[†], Michał Silarski[*], Diana Laura Sirghi[†,§], Florin Sirghi[†,§], Antonio Spallone[†], Oton Vazquez Doce[**,‡‡], Sławomir Wycech[‖‖] and Johann Zmeskal[¶]

[*]*Department of Experimental Particle Physics and Applications, Jagiellonian University, ul. Łojasiewicza 11, 30-348 Cracow, Poland*

[†]*INFN, Laboratori Nazionali di Frascati, Via Enrico Fermi 54, 00044 Frascati RM, Italy*

[‡]*Horia Hulubei National Institute of Physics and Nuclear Engineering, Street Reactorului 30, P. O. BOX MG-6, Bucharest, Magurele, Romania*

[§]*Department of Physics, Faculty of Science, University of Zagreb, Horvatovac 102a, HR-10000 Zagreb, Croatia*

[¶]*Stefan-Meyer-Institut für Subatomare Physik, Kegelgasse 27, 1030 Vienna, Austria*

[‖]*Universit degli Studi di Roma Tor Vergata, Via Cracovia snc, 00133 Rome, Italy*

[**]*Physik Department E62, Technische Universität München, James-Franck-Street 1, 85748 Garching, Germany*

[††]*Centro Ricerche Enrico Fermi – Museo Storico della Fisica e Centro Studi e Ricerche, "Enrico Fermi", Piazza del Viminale 1, 00184 Roma, Italy*

[‡‡]*Excellence Cluster "Origin and Structure of the Universe", Boltzmann Street 2, D-85748 Garching, Germany*

[§§]*RIKEN, The Institute of Physics and Chemical Research, 2-1 Hirosawa, Wako 351-0198 Saitama, Japan*

[¶¶]*Departament de Fisica Quantica i Astrofisica and Institut de Ciencies del Cosmos, Universitat de Barcelona, Marti i Franques 1, Marti i Franques 1, 08028 Barcelona, Spain*

[***]Corresponding author.

[|||]Department of Theoretical Physics,
National Center for Nuclear Research, ul. Pasteura 7,
02-093 Warsaw, Poland
[***]magdalena.skurzok@uj.edu.pl

Received 25 February 2021
Revised 5 November 2021
Accepted 28 December 2021
Published 9 February 2022

The aim of the AMADEUS collaboration is to provide new experimental constraints to the antikaon-nucleon ($\bar{K}N$) strong interaction in the regime of nonperturbative QCD, investigating the low-energy K^- hadronic interactions with light nuclei like H, ^{4}He, ^{9}Be and ^{12}C. The unique low-momentum kaon beam produced at the DAΦNE collider is ideal to study K^- nuclear captures, both at-rest and in-flight. The large acceptance KLOE detector, used as an active target, allows to achieve excellent position and momentum resolutions. In this work, a brief description of recent AMADEUS results is presented.

Keywords: Strangeness; antikaon interactions in nuclear matter.

PACS Number(s): 14.20.Jn, 14.40.−n, 13.75.Jz, 25.80.Nv

1. Introduction

The Anti-kaonic Matter at DAΦNE: An Experiment with Unraveling Spectroscopy (AMADEUS) Collaboration[1–4] investigates the low-energy K^- induced reactions in light nuclear targets (from some of the components of the KLOE detector[5] material) in order to provide experimental constraints to the nonperturbative QCD in the strangeness sector, by exploiting the low momentum ($p_K \sim 127\,\mathrm{MeV/c}$), almost monochromatic, charged kaons produced in the decay of Φ mesons at-rest at the DAΦNE accelerator.[6]

Models of low-energy strong interaction, in the strangeness sector, face difficulties mainly related to the appearance of the broad $\Lambda(1405)$ and $\Sigma(1385)$ resonances just below the $\bar{K}N$ threshold. To deal with this problem, chiral unitary models[7–13] and phenomenological potential models[14–19] were developed, leading however to contrasting predictions for the $\Lambda(1405)$ parameters and related kaonic nuclear bound states.

The $\Lambda(1405)$ resonance has spin 1/2, isospin $I = 0$, strangeness $S = -1$ and negative parity and decays into $(\Sigma\pi)^0$ through the strong interaction. Although in Particle Data Group (PDG)[20] the $\Lambda(1405)$ is listed as a four-star resonance, its nature still remains an open issue. Experiments result in observation of different masses and widths of this resonance, depending on the production channel as well as the observed decay mode.[21] The position of the $\Lambda(1405)$ reflects the strength of the $\bar{K}N$ interaction, thus influencing the possible formation of K^- multi-nucleon bound states (it is predicted that in the $\bar{K}N$ subthreshold region kaon-nucleon interaction is attractive enough to form a bound state in the isospin $I = 0$ channel).[22,23] According to the phenomenological models,[14–19] $\Lambda(1405)$ is interpreted as a pure strongly attractive $\bar{K}N$ bound state, which would imply the

formation of K^- nucleon bound states. In the chiral models,[7–13] the $\Lambda(1405)$ resonance emerges as a superposition of two states (a high-mass state located around $1420\,\mathrm{MeV/c^2}$, mainly coupled to the $\bar{K}N$ production channel and a low-mass state at $1380\,\mathrm{MeV/c^2}$, mainly coupled to the $\Sigma\pi$ channel), resulting in much less attractive K^-N interaction, which leads to the prediction of less bound kaonic nuclear states in comparison to the prediction of the phenomenological models.[23]

A strong experimental effort was devoted to the search for a K^-pp state using two main approaches: proton–proton and heavy-ion collisions (DISTO[24] and HADES[25] experiments) and in-flight or stopped K^- interactions in light nuclei (FINUDA,[26] KEK-PS E549[27] and J-PARC E15[28,29] experiments). The binding energies (B.E.) and the widths (Γ) of the lightest kaonic-nuclear cluster, K^-pp, determined from experimental data are broadly spread. In K^- induced reaction experiments, the extraction of the bound state signal is strongly affected by the yield and the shape of the competing K^- multi-nucleon absorption processes.[26,27] A signal of K^-pp kaonic nuclear bound state has been recently observed and investigated at J-PARC in the $^3\mathrm{He}(K^-, \Lambda p)n$ reaction.[29]

The activities of the AMADEUS collaboration are centered on the experimental investigations of the low-energy charged kaon-nucleon/nuclei interaction, aiming to unveil the controversial nature of the $\Lambda(1405)$ state, and deepen our understanding of the K^- single- and multi-nucleon interaction processes, and bound states formation.

This paper reports on the studies of K^- single-nucleon absorption in ^{4}He leading to the determination for the first time of the nonresonant contribution in $K^-N \to \mathrm{Y}\pi$ reaction[30] below the $\bar{K}N$ threshold which is essential for studies of the $\Lambda(1405)$ resonance properties. Moreover, we present the investigation of the K^- interactions in ^{12}C nuclei resulting in the first complete characterization of the K^- two-, three- and four-nucleon absorptions (2NA, 3NA and 4NA) in the Λp and $\Sigma^0 p$ final states and the search for K^-pp state.[31,32]

This paper is divided into five sections. The features of the DAΦNE accelerator and the KLOE detector are introduced in Sec. 2, while in Secs. 3 and 4, the data analysis and the obtained results are discussed. The summary is presented in Sec. 5.

2. The Experimental Setup

The data sample presented in this work was collected with the KLOE detection system.[5] installed at the double ring e^+e^- DAΦNE collider[6] (as it is shown in the left panel in Fig. 1) designed to work at the center of mass energy of the ϕ particle.

Double Annular Φ-factory for Nice Experiments (DAΦNE) facility delivers a monochromatic, low momentum ($\sim$127 MeV/c) charged kaon beam from the ϕ-meson decays ($\mathrm{BR(K^+K^-)} = (48.9 \pm 0.5)\%$) excellent to investigate the low-energy K^- — nucleus absorption processes. The back-to-back topology of the kaons pair production is extremely useful for the extrapolation of nonidentified kaon tracks.

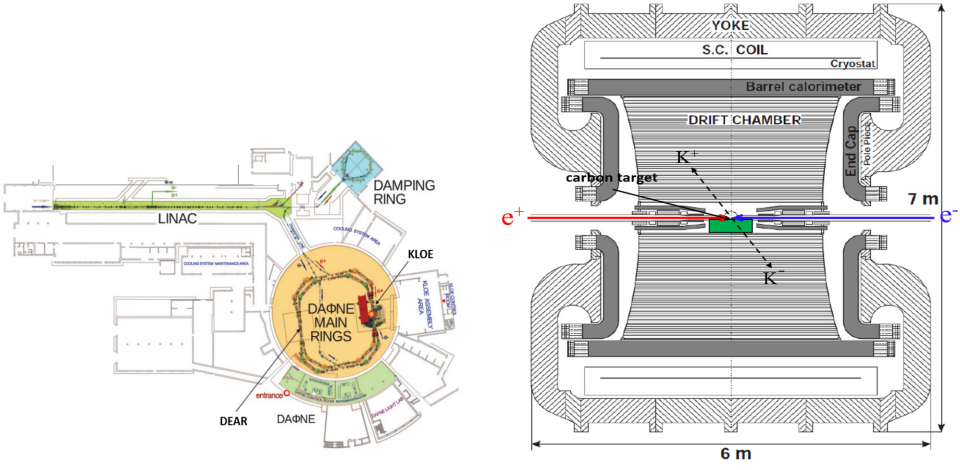

Fig. 1. (Color online) Schematic view of the DAΦNE facility with the KLOE detector in one of the interaction points (left). The cross-section of the KLOE detector with marked e^+e^- collision and $\phi \to K^+K^-$ decay (right). In green the pure graphite target is shown, used for the 2012 data taking campaign.

The KLOE (KLOng Experiment) detector, characterized by a 4π geometry, is centered around the DAΦNE interaction region. The detector consists of a large Drift Chamber (DC)[33] of cylindrical shape and a calorimeter of fine sampling lead-scintillating fibers.[34] All components are immersed in an axial magnetic field of 0.52 T, provided by a superconducting solenoid. The KLOE detector cross-section is presented in the right panel in Fig. 1.

The DC is filled with a mixture of Helium and Isobutane C_4H_{10} (90% of Helium and 10% of Isobutane in volume) and its inner radius, outer radius and length are equal to 0.25, 2 and 3.3 m, respectively. The DC entrance wall is formed of 750 μm layer of Carbon fiber and 150 μm layer of Aluminum. The particle tracks reconstruction is performed with excellent position resolution, of $\sigma_{\rho\phi} \sim 200\,\mu$m in the transverse $\rho - \phi$ plane and of $\sigma_z \sim 2$ mm along the z-axis. The transverse momentum resolution for low-momentum tracks ($p < 300$ MeV/c) is $\frac{\sigma_{p_T}}{p_T} \sim 0.4$.

The calorimeter is composed of a cylindrical barrel and two end-caps. Its volume ratio (lead/fibers/glue = 42:48:10) is optimized for a high light yield and a high efficiency for photons in the range 20–300 MeV/c. The cluster position resolution along the fibers is $\sigma_{\parallel} = 1.4\,\text{cm}\sqrt{(E/1\,\text{GeV})}$ while in the orthogonal direction is $\sigma_{\perp} = 1.4$ cm. The energy and time resolutions for photon clusters are given by $\frac{\sigma_E}{E_\gamma} = \frac{0.057}{\sqrt{(E_\gamma/1\,\text{GeV})}}$ and $\sigma_t = \frac{57ps}{\sqrt{(E_\gamma/1\,\text{GeV})}} \oplus 100$ ps.

The analyses described below refer to a sample of 1.74 fb^{-1} integrated luminosity collected by the KLOE collaboration[5] during the 2004/2005 data campaign and to the data collected in summer 2012 for a high purity carbon target (graphite) installed inside the KLOE detector, between the beam pipe and the DC inner wall.

3. Resonant and Nonresonant $Y\pi$ Transition Amplitudes Below the $\bar{K}N$ Threshold

The experimental investigation of the $\Lambda(1405)$ resonance properties is challenging since the resonance line-shape is expected to depend on both, the production mechanism and the observed decay channel. Moreover, the extraction of the $\Lambda(1405)$ invariant mass shape, in K^- induced reactions, is complicated by two biases. The first bias is the $\Sigma\pi$ invariant mass threshold imposed by the last nucleon binding energy, which for K^- capture at-rest on ^{4}He is about 1412 MeV/c^2, while for ^{12}C it is about 1416 MeV/c^2. In order to test the existence of the predicted $\Lambda(1405)$ high mass pole, which is expected to be located around 1420 MeV/c^2, it is necessary to exploit the K^- absorption in flight. Indeed for a K^- momentum of about 100 MeV/c, the $\Sigma\pi$ invariant mass threshold is shifted upwards by about 10 MeV/c^2.

Among the three $(\Sigma\pi)^0$ charge combinations, $\Sigma^0\pi^0$ represents the so-called "golden decay channel" being the best signature for the $\Lambda(1405)$ resonance free from the isospin $I = 1$ background. The $\Sigma^0\pi^0$ invariant mass spectrum from K^- captures in ^{12}C nuclei for two data samples[36] is presented in Fig. 2.[35]

The black distribution corresponds to the 2004/2005 AMADEUS data campaign, which includes both K^- captures at-rest and in-flight, while the blue distribution, obtained from 2012 data, contains mainly K^- captures at-rest. The blue and the black distributions are normalized to unity. A red line indicates the energy threshold corresponding to K^- absorption in ^{12}C at-rest. A rich sample of in-flight $K^-{}^{12}$C captures can be easily identified above the red line.

The second bias refers to the nonresonant $K^-N \to \Sigma\pi$ contribution that has to be subtracted in order to extract the $\Lambda(1405)$ shape. The nonresonant transition amplitude, below the $\bar{K}N$ threshold, was measured for the first time in the $K^-n \to \Lambda\pi^-$ channel, exploiting K^- captures on bound neutrons in ^{4}He.[30] The measured

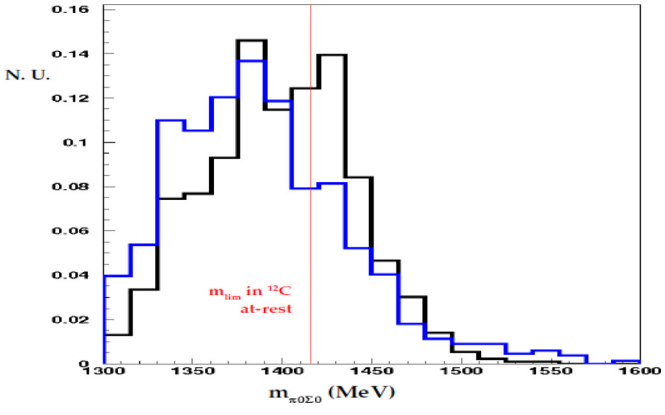

Fig. 2. (Color online) The $m_{\Sigma^0\pi^0}$ invariant mass distribution from K^- captures in the KLOE DC wall (black curve) and pure carbon graphite target (blue curve).

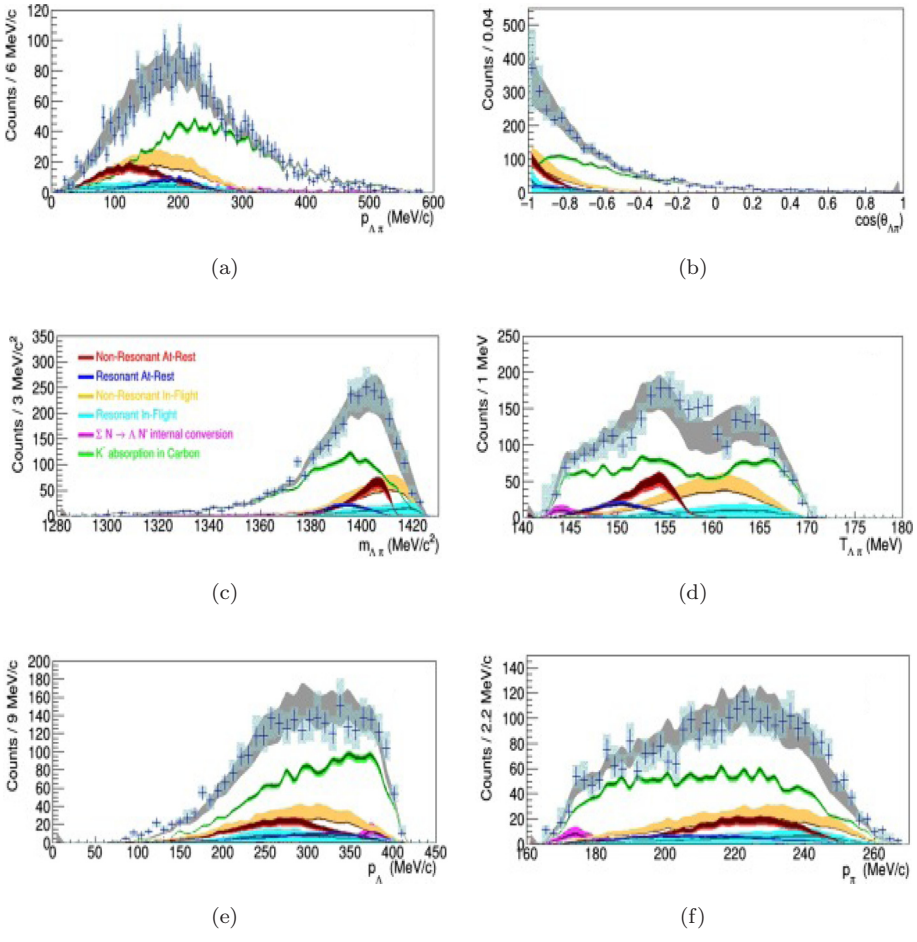

Fig. 3. (Color online) Panels (a)–(f): $p_{\Lambda\pi}$, $\cos(\theta_{\Lambda\pi})$, $m_{\Lambda\pi}$, $T_{\Lambda\pi}$, p_Λ and p_π distributions.[30] The experimental data and the corresponding statistical errors are represented by the black crosses, the systematic errors are light blue boxes. The different contributions included in the fit are shown by the colored histograms: nonresonant at-rest (red), resonant at-rest (blue), nonresonant in-flight (brown), resonant in-flight (cyan), $\Sigma N \to \Lambda N'$ internal conversion (magenta), K^- absorptions in Carbon (green). The light and dark bands correspond to systematic and statistical errors, respectively. The gray band shows the total fit with the corresponding statistical error. The plot was adapted from Ref. 30

$\Lambda\pi^-$ invariant mass, momentum and angular distributions were simultaneously fitted by means of dedicated Monte Carlo simulations based on the phenomenological K^--nucleus absorption model developed in Ref. 37. In the performed fit, shown in Fig. 3, all the contributing reactions were taken into account, namely, nonresonant processes, resonant processes, the primary production of a Σ followed by the $\Sigma N \to \Lambda N'$ conversion process and the contamination of K^{-12}C.

The analysis allowed to determine the nonresonant transition amplitude modulus which was found to be $|A_{K^-n\to\Lambda\pi^-}| = (0.334 \pm 0.018\ \text{stat.}\ ^{+0.034}_{-0.058}\ \text{syst.})$ fm

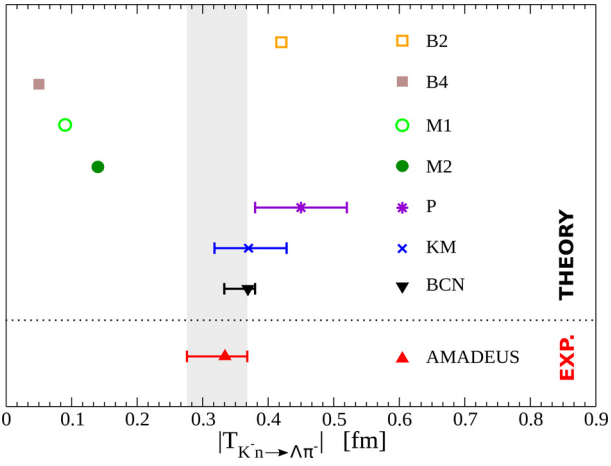

Fig. 4. Modulus of the measured nonresonant $K^-n \to \Lambda\pi^-$ transition amplitude compared with theoretical calculations, see details in the text. Figure is adapted from Ref. 43.

at $(33\pm6)\,\mathrm{MeV/c^2}$ below the $\bar{K}N$ threshold. The result (with combined statistical and systematic errors) is shown in Fig. 4 and compared with the theoretical predictions (Barcelona (BCN),[38] Prague (P),[39] Kyoto-Munich (KM),[40] Murcia (M1, M2),[41] Bonn (B2, B4)[42]) rescaled for the $K^-n \to \Sigma\pi$ transition probabilities. This measurement can be used to test and constrain the s-wave $K^-n \to \Lambda\pi^-$ transition amplitude calculations.

4. K^- Multi-Nucleon Absorption Cross-Sections and Branching Ratios in Λp and Σ^0p Final States

The possible existence of the K^-pp bound state can be investigated in the low-energy K^- induced reactions by reconstructing the proper decay channels. Recently, $\Lambda(\Sigma^0)$p final states were investigated by the AMADEUS collaboration in K^- capture processes on ^{12}C nuclei.[31,32] A complete characterization of the K^- two-, three- and four-nucleon absorption (2NA, 3NA and 4NA) processes was performed,[32] based on the phenomenological model for the K^- captures at-rest and in-flight on light nuclei described in Refs. 37 and 44. The 2NA, 3NA and 4NA absorption branching ratios (BRs) and cross-sections for low-momentum kaons in Λp and $\Sigma^0 p$ channels were determined by performing a simultaneous fit of the Λp invariant mass, Λp angular correlation, Λ and proton momenta with the simulated distributions for both Λ and Σ^0 productions followed by $\Sigma^0 \to \Lambda\gamma$ decay. For the 2NA, the contributions of both elastic final state interactions (FSI) of the primary produced hyperon and nucleon with the residual nucleus were taken into account, as well as the conversion of primary produced sigma particles ($\Sigma N \to \Lambda N'$); this allows to disentangle the quasi-free (QF) Λp and $\Sigma^0 p$ productions. The fitted spectra are shown in Fig. 5, while obtained BRs and cross-sections are summarized in Table 1.

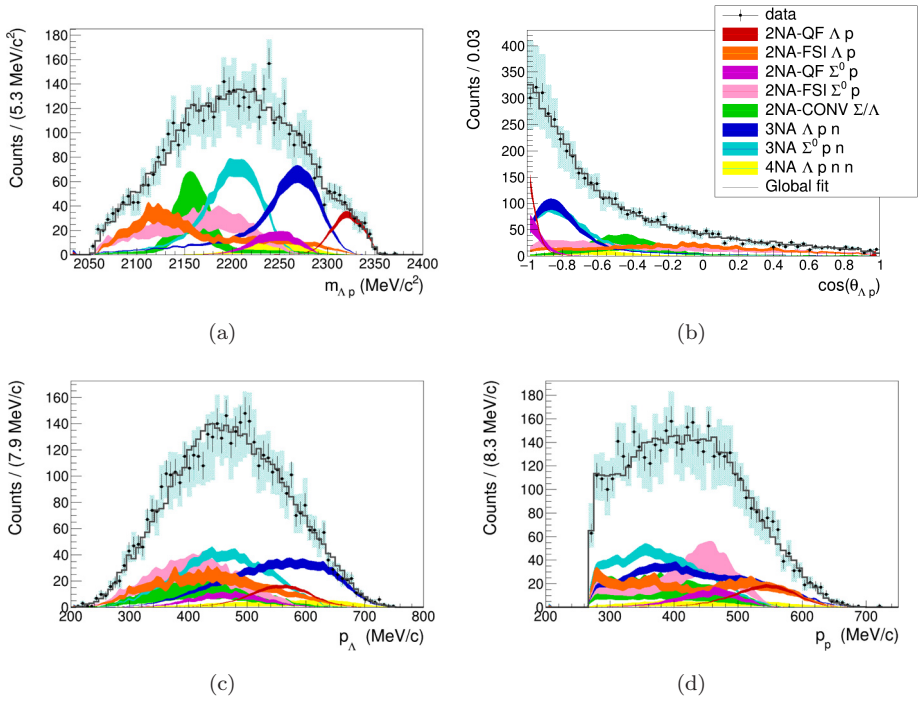

Fig. 5. Panels (a)–(f): $m_{\Lambda p}$ (Λp invariant mass), $\cos(\theta_{\Lambda p})$ (cosine of angle between Λ and proton), p_Λ (Λ momentum) and p_p (proton momentum) distributions[32] for the K^- absorption on $^{-12}$C listed in the legend. Black points represent the data, black error bars correspond to the statistical errors, cyan error bars correspond to the systematic errors. The gray line distributions represent the global fitting functions, the coloured distributions represent the different contributing processes according to the colour code reported in the legend and the widths correspond to the statistical error.

The BR of the $\Sigma^0 p$ QF production in K^- 2NA interaction is found to be greater than the Λp QF production. From the BRs in Table 1, we measure: $R = \frac{BR(K^-(pp)\to\Lambda p)}{\mathrm{BR}(K^-(\mathrm{pp})\to\Sigma^0 p)} = 0.7 \pm 0.2(\mathrm{stat.})^{+0.2}_{-0.3}(\mathrm{syst.})$. The ratio of the corresponding phase spaces is instead $R' = 1.22$. This result was interpreted in Ref. 45 and was found to be in agreement with the theoretical calculations (BCN and P models) when the in medium effect due to the Pauli blocking is considered.

The possible contribution of K^-pp bound system in Λp spectra was also investigated. It was found that K^-pp completely overlaps with the K^- 2NA-QF process, the two components can be disentangled only for narrow states ($\Gamma < 15\,\mathrm{MeV/c^2}$) which are excluded by the theoretical calculations. In the further step, in order to compare the spectra with the corresponding FINUDA measurement, back-to-back Λp events were selected ($\cos\theta_{\Lambda p} < -0.8$). As in the previous case, the obtained spectra can be completely described in terms of K^- multi-NA processes. The determined BRs are in agreement with those obtained from the fit presented in Fig. 5.

Table 1. BRs (for the K^- absorbed at-rest) and cross-sections (for the K^- absorbed in-flight) of the K^- multi-nucleon absorption processes. The K^- momentum is evaluated in the center of mass reference frame of the absorbing nucleons, thus it differs for the 2NA and 3NA processes. The statistical and systematic errors are also given. The Table is adapted from Ref. 32.

σ (mb)	@p_K (MeV/c)		
2NA-QF Λp	0.25 ± 0.02 (stat.) $^{+0.01}_{-0.02}$ (syst.)	2.8 ± 0.3 (stat.) $^{+0.1}_{-0.2}$ (syst.)	@ 128 ± 29
2NA-FSI Λp	6.2 ± 1.4 (stat.) $^{+0.5}_{-0.6}$ (syst.)	69 ± 15 (stat.) ± 6 (syst.)	@ 128 ± 29
2NA-QF Σ^0p	0.35 ± 0.09 (stat.) $^{+0.13}_{-0.06}$ (syst.)	3.9 ± 1.0 (stat.) $^{+1.4}_{-0.7}$ (syst.)	@ 128 ± 29
2NA-FSI Σ^0p	7.2 ± 2.2 (stat.) $^{+4.2}_{-5.4}$ (syst.)	80 ± 25 (stat.) $^{+46}_{-60}$ (syst.)	@ 128 ± 29
2NA-CONV Σ /Λ	2.1 ± 1.2 (stat.) $^{+0.9}_{-0.5}$ (syst.)	—	
3NA Λpn	1.4 ± 0.2 (stat.) $^{+0.1}_{-0.2}$ (syst.)	15 ± 2 (stat.) ± 2 (syst.)	@ 117 ± 23
3NA Σ^0pn	3.7 ± 0.4 (stat.) $^{+0.2}_{-0.4}$ (syst.)	41 ± 4 (stat.) $^{+2}_{-5}$ (syst.)	@ 117 ± 23
4NA Λpnn	0.13 ± 0.09 (stat.) $^{+0.08}_{-0.07}$ (syst.)	—	
Global $\Lambda(\Sigma^0)$p	21 ± 3 (stat.) $^{+5}_{-6}$ (syst.)	—	

5. Summary

We presented in this work the AMADEUS investigations of the low-energy interaction between K^- and nucleons/nuclei in light nuclear targets providing input for a better understanding of the nonperturbative quantum chromodynamics QCD in the strangeness sector. Studies of the K^-n single nucleon absorption in ^{4}He allowed to characterize for the first time the nonresonant $K^-N \to Y\pi$ production below the $\bar{K}N$ threshold which is crucial for the investigation of the $\Lambda(1405)$ characteristics. Studies of low-energy K^- captures on a solid carbon target result in a complete characterization of the two-, three- and four-nucleon absorptions in the Λp and $\Sigma^0 p$ final states (BRs and cross-sections). Moreover, it was found that the contribution from a possible K^-pp bound state completely overlaps with the K^- 2NA-QF process.

Acknowledgments

We acknowledge the KLOE/KLOE-2 Collaboration for their support and for having provided us the data and the tools to perform the analysis presented in this paper. We acknowledge the Centro Ricerche Enrico Fermi — Museo Storico della Fisica e Centro Studi e Ricerche "Enrico Fermi", for the Project PAMQ. Part of this work was supported by the Austrian Science Fund (FWF): [P24756-N20]; Austrian Federal Ministry of Science and Research BMBWK 650962/0001 VI/2/2009; the Croatian Science Foundation, Under Project 8570; Polish National Science Center through Grant No. UMO-2016/21/D/ST2/01155; EU Horizon 2020 STRONG-2020-No. 824093 Project.

References

1. R. Del Grande *et al.*, *J. Phys.*: *Conf. Ser.* **1643** (2020) 012081.

2. M. Skurzok *et al.*, *Springer Proc. Phys.* **238** (2020) 937.
3. M. Skurzok *et al.*, *JPS Conf. Proc.* **26** (2019) 023011.
4. C. Curceanu *et al.*, *Acta. Phys. Pol. B* **46** (2015) 203.
5. F. Bossi *et al.*, *Riv. Nuovo Cim.* **31** (2008) 531.
6. A. Gallo *et al.*, *Conf. Proc. C* **060626** (2006) 604.
7. A. Dote, T. Hyodo and W. Weise, *Phys. Rev. C* **79** (2009) 014003.
8. A. Dote, T. Inoue and T. Myo, *Phys. Lett. B* **784** (2018) 405.
9. N. Barnea, A. Gal and E. Z. Liverts, *Phys. Lett. B* **712** (2012) 132.
10. Y. Ikeda, H. Kamano and T. Sato, *Prog. Theor. Phys.* **124** (2010) 533.
11. P. Bicudo, *Phys. Rev. D* **76** (2007) 031502.
12. M. Bayar and E. Oset, *Nucl. Phys. A* **914** (2013) 349.
13. T. Sekihara, E. Oset and A. Ramos, *Prog. Theor. Exp. Phys.* **2016** (2016) 12.
14. Y. Akaishi and T. Yamazaki, *Phys. Rev. C* **65** (2002) 044005.
15. Y. Ikeda and T. Sato, *Phys. Rev. C* **76** (2007) 035203.
16. S. Wycech and A. M. Green, *Phys. Rev. C* **79** (2009) 014001.
17. N. V. Shevchenko, A. Gal and J. Mares, *Phys. Rev. Lett.* **98** (2007) 082301.
18. J. Revai and N. V. Shevchenko, *Phys. Rev. C* **90** (2014) 034004.
19. S. Maeda, Y. Akaishi and T. Yamazaki, *Proc. Jpn. Acad. B* **89** (2013) 418.
20. Particle Data Group (P. A. Zyla *et al.*), *Prog. Theor. Exp. Phys.* **2020** (2020) 083C01.
21. T. Hyodo and D. Jido, *Prog. Part. Nucl. Phys.* **67** (2012) 55.
22. S. Wycech, *Nucl. Phys. A* **450** (1986) 399c.
23. Y. Akaishi and T. Yamazaki, *Phys. Lett. B* **535** (2002) 70.
24. M. Maggiora *et al.*, *Nucl. Phys. A* **835** (2010) 43.
25. G. Agakishiev, *Phys. Lett. B* **742** (2015) 242.
26. M. Agnello *et al.*, *Phys. Rev. Lett.* **94** (2005) 212303.
27. T. Suzuki *et al.*, *Mod. Phys. Lett. A* **23** (2008) 2520.
28. Y. Sada *et al.*, *Prog. Theor. Exp. Phys.* **2016** (2016) 051D01.
29. S. Ajimura *et al.*, *Phys. Lett. B* **789** (2019) 620.
30. K. Piscicchia *et al.*, *Phys. Lett. B* **782** (2018) 339.
31. O. Vazques Doce *et al.*, *Phys. Lett. B* **758** (2016) 134.
32. R. Del Grande *et al.*, *Eur. Phys. J. C* **79** (2019) 190.
33. KLOE Collab. (M. Adinolfi *et al.*), *Nucl. Instrum. Methods A* **488** (2002) 51.
34. KLOE Collab. (M. Adinolfi *et al.*), *Nucl. Instrum. Methods A* **482** (2002) 364.
35. K. Piscicchia *et al.*, *Acta. Phys. Pol. B Proc. Suppl.* **11** (2018) 609.
36. K. Piscicchia, Ph.D. Thesis "L(1405) measurement through the decay to S0p0, resulting from K-meson absorption on ^{4}He and ^{12}C, with the KLOE detector", Department of Physics of Universita degli Studi Roma TRE.
37. K. Piscicchia, S. Wycech and C. Curceanu, *Nucl. Phys. A* **954** (2016) 75.
38. A. Feijoo, V. Magas and A. Ramos, *Phys. Rev. C* **99** (2019) 035211.
39. A. Cieplý and J. Smejkal, *Nucl. Phys. A* **881** (2012) 115.
40. Y. Ikeda, T. Hyodo and W. Weise, *Nucl. Phys. A* **881** (2012) 98.
41. Z. H. Guo and J. A. Oller, *Phys. Rev. C* **87** (2013) 035202.
42. M. Mai and U. G. Meissner, *Eur. Phys. J. A* **51** (2015) 30.
43. A. Feijoo, V. K. Magas and A. Ramos, *AIP Conf. Proc.* **2130** (2019) 040013.
44. R. Del Grande, K. Piscicchia and S. Wycech, *Acta Phys. Pol. B* **48** (2017) 1881.
45. J. Hrtankova and A. Ramos, *Phys. Rev. C* **101** (2020) 035204.